Stability Analysis of Jets in Crossflow

Marc Regan

Aerospace Engineering & Mechanics
University of Minnesota
107 Akerman Hall
110 Union St SE
Minneapolis, Minnesota 55455-0153
United States of America
rega0113@umn.edu

Krishnan Mahesh

Aerospace Engineering & Mechanics
University of Minnesota
107 Akerman Hall
110 Union St SE
Minneapolis, Minnesota 55455-0153
United States of America
kmahesh@umn.edu

ABSTRACT

Jets in crossflow (JICFs), or transverse jets, are a canonical flow where a jet of fluid is injected normal to a crossflow. The interaction between the incoming flat-plate boundary layer and the jet is dependent on the Reynolds number ($Re = \bar{v}_j D/v$), based on the average velocity ($\bar{v}_{jet}$) at the jet exit and the diameter (D), as well as the jet-to-crossflow ratio ($R = \bar{v}_{jet}/u_\infty$). Megerian *et al.* (2007) performed experiments at $Re = 2000$ and collected vertical velocity spectra along the upstream shear-layer. They observed that the upstream shear-layer transitions from absolutely to convectively unstable between $R = 2$ and $R = 4$. Using an unstructured, incompressible, direct numerical simulation (DNS) solver, Iyer & Mahesh (2016) performed simulations matching the experimental setup of Megerian *et al.* (2007). Vertical velocity spectra taken along the upstream shear-layer from simulation show good agreement with experiment, marking the first high-fidelity simulation able to fully capture the complex shear-layer instabilities in low speed jets in crossflow. Iyer & Mahesh (2016) proposed an analogy to counter-current mixing along the leading edge shear-layer to explain the transition from an absolute to convective instability. In addition, Iyer & Mahesh (2016) performed dynamic mode decomposition (DMD) of the velocity field, which reproduced the dominant frequencies obtained from the upstream shear-layer spectra.

In the present work, the stability of JICFs is studied when $R = 2$ and $R = 4$ using global linear stability analysis (GLSA) (i.e Tri-Global linear stability analysis), where the baseflow is fully three-dimensional. A variant of the implicitly restarted Arnoldi method (IRAM) in conjunction with a time-stepper approach is implemented to efficiently calculate the leading eigenvalues and their associated eigenmodes. The Strouhal frequencies ($St = fD/v_{jet}$), based on the peak velocity (v_{jet}) at the jet exit and the diameter (D), from linear stability analysis are compared with experiments (Megerian *et al.*, 2007) and simulations (Iyer & Mahesh, 2016). The eigenmodes are analyzed and show evidence that supports the transition from an absolutely to convectively unstable flow. Additionally, the adjoint sensitivity of the upstream shear-layer is studied for the case when $R = 2$. The location of the most sensitive areas is shown to be localized to the upstream side of the jet nozzle near the jet exit. The wavemaker for the upstream shear-layer is then calculated using the direct and adjoint eigenmodes for case $R = 2$. The results further justify the absolutely unstable nature of the region near the upstream side of the jet nozzle exit.

INTRODUCTION

A jet in crossflow (JICF) is a canonical flow where a wall-normal jet of fluid interacts with an incoming crossflow. The flat-plate boundary layer created by the crossflow interacts with the jet to create a set of complex vortical structures. Shear-layer vortices and the Kelvin-Helmholtz instability often form on the upstream side of the jet path. Further downstream, a counter-rotating vortex pair (CVP) dominates the jet cross section (Kamotani & Greber, 1972; Smith & Mungal, 1998). Horseshoe vortices are also formed near the wall, just upstream of the jet exit (Krothapalli *et al.*, 1990; Kelso & Smits, 1995). These travel downstream as they begin to tilt upward and form wake vortices during 'separation events' (Fric & Roshko, 1994) caused by the near-wall adverse pressure gradient. Wake vortices have long been studied in the literature (Kelso *et al.*, 1996; Eiff *et al.*, 1995; McMahon *et al.*, 1971; Moussa *et al.*, 1977). Transverse jets are found in many real-world engineering applications, such as: film cooling, vertical and/or short take-off and landing (V/STOL) aircraft, thrust vectoring, and gas turbine dilution jets. Reviews by Margason (1993), Karagozian (2010) and Mahesh (2013) describe most of the research over the last seven decades.

Low-speed incompressible isodensity JICFs may be characterized by the following: the jet Reynolds number $Re = \bar{v}_{jet}D/v_{jet}$, based on the average jet exit velocity ($\bar{v}_{jet}$), the jet diameter (D), and the kinematic viscosity of the jet (v_{jet}); the jet-to-crossflow velocity ratio $R = \bar{v}_{jet}/u_\infty$. The jet-to-crossflow velocity ratio may also be defined as $R^* = v_{jet,max}/u_\infty$, based on the maximum velocity at the jet exit.

Megerian *et al.* (2007) experimentally studied low-speed JICFs at Reynolds numbers of 2000 and 3000 over a range of jet-to-crossflow ratios ($1 \leq R \leq 10$). Vertical velocities were collected at various probe points along the upstream shear-layer to compute velocity spectra. They observed that this region transitions from absolutely to convectively unstable between $R = 2$ and $R = 4$. Megerian *et al.* (2007) showed that when $R = 2$ the upstream shear-layer has a strong pure-tone mode at a single Strouhal number ($St = fD/v_{jet,max}$), based on the jet exit diameter (D) and the maximum velocity at the jet exit ($v_{jet,max}$). This behavior is consistent with an absolutely unstable flow, where an instability grows at the point of origin and travels downstream. On the contrary, when $R = 4$, Megerian *et al.* (2007) observed that instabilities associated with the upstream shear-layer were not only weaker, but subharmonics formed further downstream. These observations are consistent with a convectively unstable flow, where instabilities grow as they travel downstream.

Davitian *et al.* (2010) further characterized the transition from absolute to convective instability by examining the spatial development of the fundamental and subharmonic modes that form further downstream along the shear-layer. Additionally, Davitian *et al.* (2010) examined the response of the upstream shear-layer to strong sinusoidal forcing. They show clear evidence that for flush JICFs, the near-field shear-layer becomes globally unstable when $R^* \leq 3$ at $Re = 2000$. Furthermore, evidence is shown that suggests strong sinusoidal forcing applied to a globally unstable JICF can replace one mode for another with little impact on the overall behavior. These results build on the prior studies of M'Closkey *et al.* (2002), who

suggested that strong sinusoidal forcing has little impact on the behavior of JICFs when compared to square-wave forcing. The results by Davitian *et al.* (2010) and M'Closkey *et al.* (2002) highlight the importance of understanding the stability transition of the upstream shear-layer due to the effect it has on the overall controllability of JICFs.

DNSs by Iyer & Mahesh (2016) match the same experimental setup as Megerian *et al.* (2007) for $R = 2, 4$ at $Re = 2000$. Good agreement was shown between simulation and experiment for both the time-averaged flow, as well as the vertical velocity spectra obtained along the upstream shear-layer. Dynamic mode decomposition (DMD) was shown to capture to complex flow dynamics at the same Strouhal numbers obtained from vertical velocity spectra. Iyer & Mahesh (2016) proposed an analogy to counter-current mixing layers. They assumed the upstream shear-layer acted as a counter-current shear-layer, and therefore characterized the stability using the classic parallel flow analysis by Huerre & Monkewitz (1985). A velocity ratio,

$$Q = \frac{V_1 - V_2}{V_1 + V_2} \qquad (1)$$

is defined, where V_1 and V_2 are the velocities for the two mixing layers. Huerre & Monkewitz (1985) show that for $Q > 1.315$ a mixing layer is absolutely unstable, and for $Q < 1.315$ it is convectively unstable. Iyer & Mahesh (2016) show that in their simulations $Q = 1.44$ when $R = 2$ and $Q = 1.20$ when $R = 4$. This is consistent with the stability transition for JICFs in the literature, and may suggest that the mechanism that drives stability for free shear-layers may also govern the stability for more complex flows like JICFs.

The stability of JICFs have been studied using linear stability analysis (LSA) by Bagheri *et al.* (2009). Their analysis marks the first simulation-based Tri-Global LSA of a three-dimensional flowfield assuming no homogeneous directions. Throughout the present work, this type of analysis will be referred to as Global LSA (GLSA). Bagheri *et al.* (2009) studied the stability of JICFs at $R^* = 3$ at $Re_{\delta_0^*} = u_\infty \delta_0^* / \nu = 165$, which is based on the displacement thickness δ_0^* at the inlet of the crossflow. GLSA was performed on a steady baseflow obtained using selective frequency damping (SFD) (Åkervik *et al.*, 2006). In their analysis, the jet nozzle was not included, and instead a parabolic velocity profile was prescribed at the jet nozzle exit. The most unstable high-frequency modes were found along the upstream shear-layer, whereas low-frequency wake modes were found downstream. The frequency of the upstream shear-layer was not far from the non-linear shedding frequency; however, the wake mode frequency was far from the non-linear wake frequency. It was suggested by Bagheri *et al.* (2009) that the difference could be related to the differences between the SFD solution used in GLSA and the time-averaged solution.

Peplinski *et al.* (2015) studied JICFs at low values of R in the range between 1.5 and 1.6 using GLSA as well as global adjoint sensitivity analysis (GASA). GASA provides valuable sensitivity information about the flowfield through the use of the adjoint to the linearized Navier-Stokes equations. Peplinski *et al.* (2015) prescribe a super-exponential Gaussian function at the jet exit. Their results show large streamwise separation between the direct and adjoint eigenmodes induced by the flow advection. Additionally, the adjoint eigenmode is located on the jet exit boundary. This suggests a large sensitivity to the jet exit boundary condition, and may point to a necessary inclusion of the jet nozzle in this simulation.

The present work studies the stability of JICFs using GLSA for $R = 2, 4$ and GASA for $R = 2$ of the turbulent mean flow. The same nozzle used in experiments by Megerian *et al.* (2007) is used in our

simulations. The nozzle is designed to provide a top-hat profile at the jet exit. Performing GLSA, GASA, or even DNS, of JICF is very computationally expensive. There are 80 million elements in the grid used for the present work, which translates to an eigenvalue problem with a dimension of 240 million. Therefore, a variation of the Arnoldi iteration method (Arnoldi, 1951) is used to efficiently calculate the direct and adjoint eigenvalue spectra and the associated eigenmodes. Once the direct (GLSA) and adjoint (GASA) solutions are known, the wavemaker is computed for the upstream shear-layer to highlight the regions that are most sensitive to localized feedback. A brief discussion section provides conclusion to the presented results.

NUMERICAL METHODOLOGY

The incompressible Navier-Stokes (N-S) equations may be written as,

$$\frac{\partial u_i}{\partial t} + \frac{\partial}{\partial x_j} u_i u_j = -\frac{\partial p}{\partial x_i} + \nu \frac{\partial^2 u_i}{\partial x_j \partial x_j}$$
$$\frac{\partial u_i}{\partial x_i} = 0, \qquad (2)$$

where ν is the kinematic viscosity of the fluid. Equations 2 are solved using an unstructured, finite-volume algorithm developed by Mahesh *et al.* (2004). The algorithm has been validated for a number of complex flows, including: a gas turbine combustor (Mahesh *et al.*, 2004), free jet entrainment (Babu & Mahesh, 2004), and transverse jets (Muppidi & Mahesh, 2005, 2007, 2008; Sau & Mahesh, 2007, 2008). The spatial discretization technique focuses on conserving discrete energy, which by design ensures that the flux of kinetic energy only has contributions from the boundary elements. These properties of the numerical algorithm ensure high-fidelity simulation of complex flows at high Reynolds numbers without added numerical dissipation. Adams-Bashforth second-order time integration is used to advance the predictor velocities through the momentum equation. Next, the Poisson equation for pressure is derived by taking the divergence of the momentum equation and satisfying conservation of mass. The pressure field is then used to project the velocity field to be divergence-free.

The N-S equations (eq. 2) can be linearized about a base state,

$$\overline{u}_i = \overline{u}_i(x, y, z)$$
$$\overline{p} = \overline{p}(x, y, z) \qquad (3)$$

which varies arbitrarily in space. By decomposing the flowfield into the known base state ($\overline{u}_i$) plus some $O(\varepsilon)$ perturbation ($\tilde{u}_i$), and neglecting the ε^2 terms, we arrive at the linearized Navier-Stokes (LNS) equations:

$$\frac{\partial \tilde{u}_i}{\partial t} + \frac{\partial}{\partial x_j} \tilde{u}_i \overline{u}_j + \frac{\partial}{\partial x_j} \overline{u}_i \tilde{u}_j = -\frac{\partial \tilde{p}}{\partial x_i} + \nu \frac{\partial^2 \tilde{u}_i}{\partial x_j \partial x_j}$$
$$\frac{\partial \tilde{u}_i}{\partial x_i} = 0 \qquad (4)$$

If our interest is in the long-time behavior of $\tilde{u}_i$, then solutions to the LNS (eq. 4) are of the form:

$$\tilde{u}_i(x, y, z, t) = \hat{u}_i(x, y, z) e^{\omega t} + \text{c.c} \qquad (5)$$

where ω and $\hat{u}_i$ can be complex. The real part ($\text{Re}(\omega)$) is the growth/damping rate and the imaginary part ($\text{Im}(\omega)$) is the temporal frequency of $\hat{u}_i$. By substituting in the ansantz (eq. 5), the

LNS equations (eq. 4) reduce to a linear eigenvalue problem, where ω is the eigenvalue and $\hat{u}_i$ is the eigenmode.

To arrive at the adjoint LNS (ALNS) equations we define the same Lagrangian identity as Hill (1995):

$$\frac{\partial \tilde{u}_i^\dagger}{\partial t} + \frac{\partial}{\partial x_j}\tilde{u}_i^\dagger \overline{u}_j - \tilde{u}_j^\dagger \frac{\partial}{\partial x_i}\overline{u}_j = -\frac{\partial \tilde{p}^\dagger}{\partial x_i} - \nu \frac{\partial^2 \tilde{u}_i^\dagger}{\partial x_j \partial x_j}$$
$$\frac{\partial \tilde{u}_i^\dagger}{\partial x_i} = 0 \qquad (6)$$

The ALNS equations are integrated backwards in time and provide sensitivity information for the corresponding LNS equations. By applying the same ansantz (eq. 5), the ALNS reduce to an eigenvalue problem that can be solved using the same numerical techniques as the direct problem. Additionally, the eigenvalues for the direct and adjoint problems coincide with each other. Therefore each direct eigenmode has a corresponding adjoint eigenmode that provides sensitivity information.

The adjoint velocity field defines the sensitivity of the associated direct mode to an unsteady point force aligned with the adjoint velocity vector. This provides valuable sensitivity information in regards to the underlying flow physics and points to locations in the domain that are sensitive to control.

When performing GLSA and GASA, the rank of the eigenvalue problem can be $O(10^6 - 10^8)$. Solving eigenvalue problems of this size often prohibits the use of direct methods. In the present work, we use an extension of the Arnoldi iteration method (Arnoldi, 1951) called the Implicitly Restarted Arnoldi Method (IRAM). This method is matrix-free, which, in conjunction with a time-stepper approach, only requires the solution of an LNS time integrator to solve for the leading eigenvalues.

A turbulent mean flow can be used as the base state for GLSA and GASA. This choice of base state is a solution to the Reynolds-averaged N-S equations. Therefore, a non-linear Reynolds stress term is effectively added to the LNS and ALNS equations when the baseflow equations are subtracted. A mode-dependent Reynolds stress term is therefore present in the associated eigenvalue problems. A scale-separation argument first introduced by Crighton & Gaster (1976), and more recently by Jordan & Colonius (2013), can be used to justify when the mode-dependent Reynolds stress term can be assumed negligible. Only for the eigenmodes of interest, which are typically large-scale and low frequency when compared to turbulent scales, must the Reynolds stress term be shown negligible. For highly turbulent flows there can be multiple orders of magnitude separating the length (η) and time (t_η) scales of turbulent motions with the length (L) and time (t_L) scales for the motions of interest. The Kolmogorov scales, as seen in Pope (2000) determine the scale-separation as follows:

$$L/\eta = Re^{3/4} \qquad (7)$$
$$t_L/t_\eta = Re^{1/2} \qquad (8)$$

If the scale-separation argument holds, performing GLSA and GASA with a turbulent mean flow can provide valuable physical insight with respect to stability and sensitivity.

RESULTS

Figure 1 shows the computational setup. The inflow boundary condition is a laminar Blasius boundary layer profile. The grid is shown in Figure 1b-d and is identical to the grid used by Iyer & Mahesh (2016). Additionally, the boundary layer profiles used
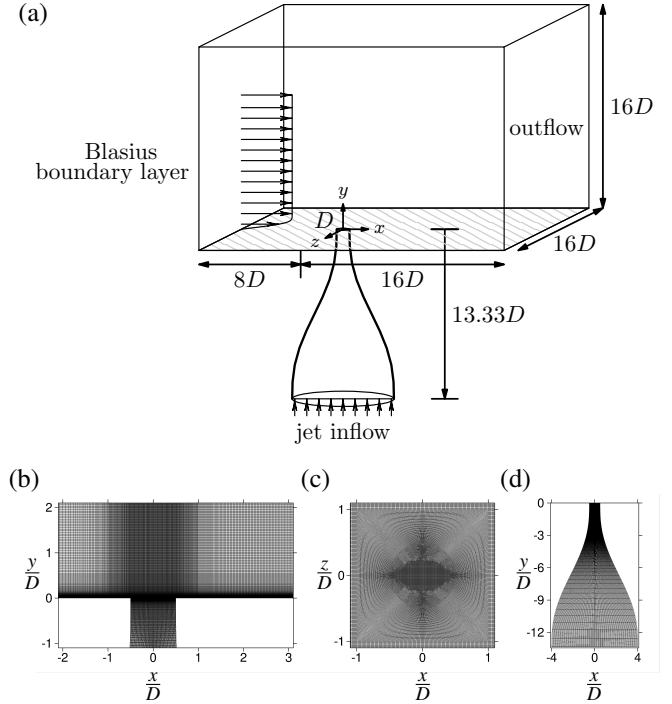

Figure 1. Shown is the computational domain for the jet in crossflow (a). The origin is located at the center of the jet nozzle exit. The nozzle shape is modeled by a 5th-order polynomial and matches the nozzle used in experiments by Megerian *et al.* (2007). Uniform flow is prescribed at the jet inflow, whereas a Blasius boundary layer is prescribed at the leftmost inflow boundary condition. Three cross-sectional views of the computational grid that show detailed views of the symmetry plane (a), jet exit (b), as well as the jet nozzle (c). This grid is composed of 80 million elements.

in the present work are the same as those used by Iyer & Mahesh (2016). The profiles have been shown to be in good agreement with experiments at $x/D = -5.5$. The jet nozzle shape is modeled by the same 5th-order polynomial used in experiments (Megerian *et al.*, 2007) and is included in all simulations. Including the nozzle has been shown (Iyer & Mahesh, 2016) to play a crucial role in the setup of the mean flow near the jet exit, which effects the stability characteristics of the flow. The jet exit diameter (D) is 3.81 mm and the average velocity at the jet exit ($\overline{v}_{jet}$) is 8 m s^{-1}. Additional simulation details are outlined in Table 1; they match the conditions used in experiments and computations by Megerian *et al.* (2007) and Iyer & Mahesh (2016), respectively.

The scale-separation argument provides the following results for JICFs:

$$L/\eta = Re^{3/4} \approx 300 \qquad (9)$$
$$t_L/t_\eta = Re^{1/2} \approx 45 \qquad (10)$$

This shows that one or more orders of magnitude separate the time and length scales of turbulent motions and the motions of interest. Therefore, turbulent mean flow solutions are a valid baseflow choice and are used as the baseflows in GLSA for the present work.

Figure 2 shows the results from GLSA for cases $R = 2$ ($R2$) and $R = 4$ ($R4$). The eigenvalues have been non-dimensionalized by $2\pi v_{jet,max}/D$ so that the growth rate is $\text{Re}(\omega)D/(2\pi v_{jet,max})$ and the Strouhal number is $\text{Im}(\omega)D/(2\pi v_{jet,max})$. The vertical dash-dotted lines in the Figure 2 highlight the Strouhal numbers recovered from DNS by Iyer & Mahesh (2016), and show good agree-

Table 1. Simulation parameters R and R^* are jet-to-crossflow ratios based on the average jet exit velocity and the peak jet exit velocity, respectively. Jet to crossflow ratios (R) of 2 and 4 are studied at a Reynolds number of 2000, based on the average velocity ($\bar{v}_{jet}$) at the jet exit and the jet exit diameter (D). Also shown is an alternative jet to crossflow ratio (R^*), based on the jet exit peak velocity ($v_{jet,max}$). The momentum thickness of the laminar crossflow boundary layer is described at the jet exit when the jet is turned off.

Case	R	R^*	Re	θ_{bl}/D
$R2$	2	2.44	2000	0.1215
$R4$	4	4.72	2000	0.1718

ment with the upstream shear-layer eigenmodes (circled in Figure 2). Additionally, the associated eigenmodes are shown in Figure 3 ($R2$) and Figure 4 ($R4$), and show good agreement with the DMD modes by Iyer & Mahesh (2016).

For case $R2$, Figure 3 shows that there are two main groups of eigenmodes; the shear-layer mode and the wake modes. The upstream shear-layer mode originates near the jet exit and oscillates at a frequency very close the what is observed in DNS and experiments. This eigenmode extends downstream beyond the collapse of the potential core. Therefore the eigenmode is growing as it travels downstream but also growing at the point of origin. This behavior near the jet exit is characteristic of an absolutely unstable flow. The group of downstream wake modes highlight the connection between the near-wall motions and the jet wake.

The Reynolds stresses present in the turbulent mean flow show up in GLSA as stationary eigenmodes (i.e. non-oscillatory). This is because the Reynolds stresses act as a steady forcing term in the LNS equations. Therefore, the stationary eigenmodes are not relevant to the present work and are not included.

For case $R4$, Figure 4 shows the two groups of eigenmodes, consisting of the downstream and upstream shear-layers. Two of the high-frequency downstream shear-layer eigenmodes are the most unstable and therefore play an important role in the stability. These high-frequency modes span a range of frequencies and interact with the upstream shear-layer after the collapse of the potential core. This may explain why there are different frequencies present along upstream shear-layer in DNS and experiment when $R = 4$. Additionally, the upstream shear-layer mode oscillates at a Strouhal number that is in very good agreement with experiments and DNS. When compared to case $R2$, the upstream shear-layer mode for $R4$ originates further away from the jet exit. This behavior near the origin the of shear-layer mode is consistent with a convective instability where the instability travels downstream, but does not grow at the point of origin.

GASA has been performed for case $R2$ for the leading instability (i.e. upstream shear-layer). Figure 5 shows the leading adjoint eigenmode with an associated eigenvalue $\omega = 0.050 \pm i0.61$, which coincides with the leading direct eigenmode. Therefore, this adjoint eigenmode provides sensitivity information about the direct mode. Looking at Figure 5 shows that the adjoint eigenmode is localized near the inside the jet nozzle on the upstream side. This implies that the direct upstream shear-layer eigenmode is most sensitive to forcing at this location.

The wavemaker associated with the upstream shear-layer can be computed by correlating the direct and adjoint eigenmodes. Figure 6 shows the wavemaker which defines the region that is most
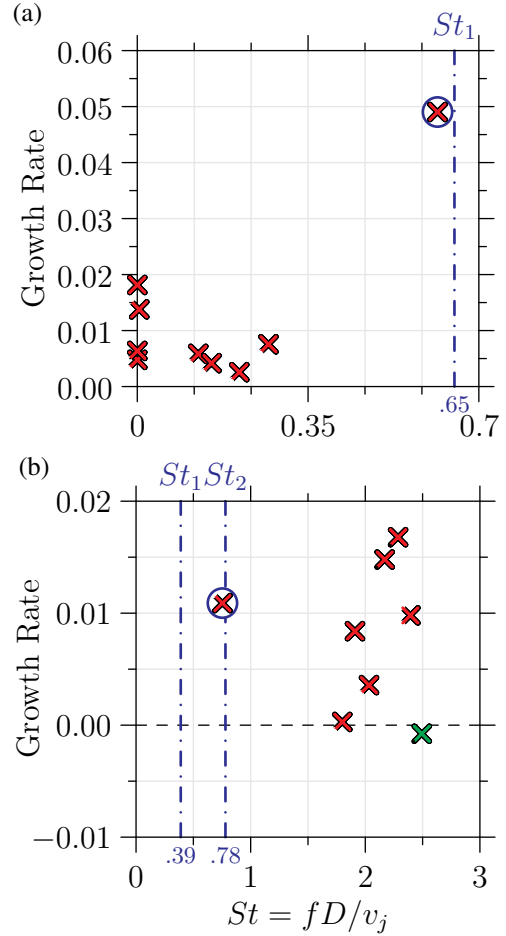

Figure 2. GLSA eigenvalue spectrum for JICF at a Reynolds number of 2000 for case $R2$ (a) and $R4$ (b). The growth rates and Strouhal numbers are normalized appropriately. Vertical velocity spectra from Iyer & Mahesh (2016) are shown (dash-dotted lines) for comparison. Note that $St_2 = 1.3$ is not shown in (a) as it would obscure the low frequency results. The eigenvalues with positive growth rates are unstable.

sensitive to localized feedback. It is clear that two lobes make up the wavemaker; one on the upstream side of the shear-layer and one on the downstream side that extends into the jet nozzle. Perturbations to the base state that travel through the wavemaker are subject to localized feedback. Therefore, perturbing just inside jet nozzle on the upstream side, or the boundary layer just upstream of the jet exit, could cause localized feedback to amplify the direct upstream shear-layer eigenmode (Figure 3a). Additionally, the location of the wavemaker confirms the absolutely unstable nature of the flow in the vicinity of the jet exit because the wavemaker is located at the origin of the direct upstream shear-layer eigenmode.

CONCLUSIONS

Performing GLSA of low-speed JICFs, using turbulent mean flows as the base states, has been shown to produce upstream shear-layer eigenmodes that oscillate at frequencies close to those observed in experiments (Megerian *et al.*, 2007) and simulations (Iyer & Mahesh, 2016) for R values of 2 and 4. Additional unstable eigenmodes have been shown that occupy the wake for $R = 2$ that dominate far downstream. Also, for case $R4$, the downstream shear-layer modes have been shown to be more unstable than upstream shear-layer modes and span a range of frequencies. The transition from
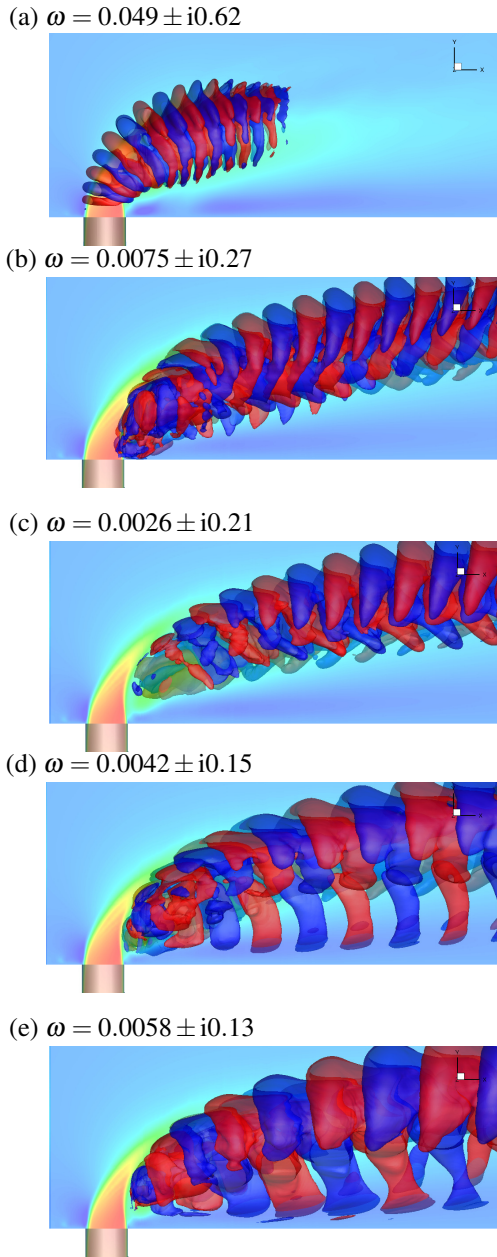
(a) $\omega = 0.049 \pm i0.62$

(b) $\omega = 0.0075 \pm i0.27$

(c) $\omega = 0.0026 \pm i0.21$

(d) $\omega = 0.0042 \pm i0.15$

(e) $\omega = 0.0058 \pm i0.13$

Figure 3. Real part of the eigenmodes for case $R2$ are shown with positive and negative isocontours of $\tilde{u}$ and $\bar{v}$ contours of the base state in the background. Mode (a) corresponds to the most unstable and highest frequency upstream shear-layer mode. Modes (b-e) are lower frequency and originate near the downstream shear-layer and travel far downstream. Modes (d) and (e) also show a connection between near-wall motions and motions in the jet wake. Note that the zero-frequency modes are not shown.

absolute to convective instability observed in simulations and experiments have been further justified through the use of GLSA.

GASA analysis for case $R2$ has been shown to coincide with the GLSA spectrum. This allows the conclusion that the upstream shear-layer eigenmode is sensitive to forcing along the upstream side of the jet nozzle close to the jet exit. Furthermore, the computation of the wavemaker shows that the upstream shear-layer direct mode is subject to localized feedback near its point of origin. This further justifies the conclusion that in the vicinity of the jet exit, case $R2$ behaves as an absolutely unstable flow.
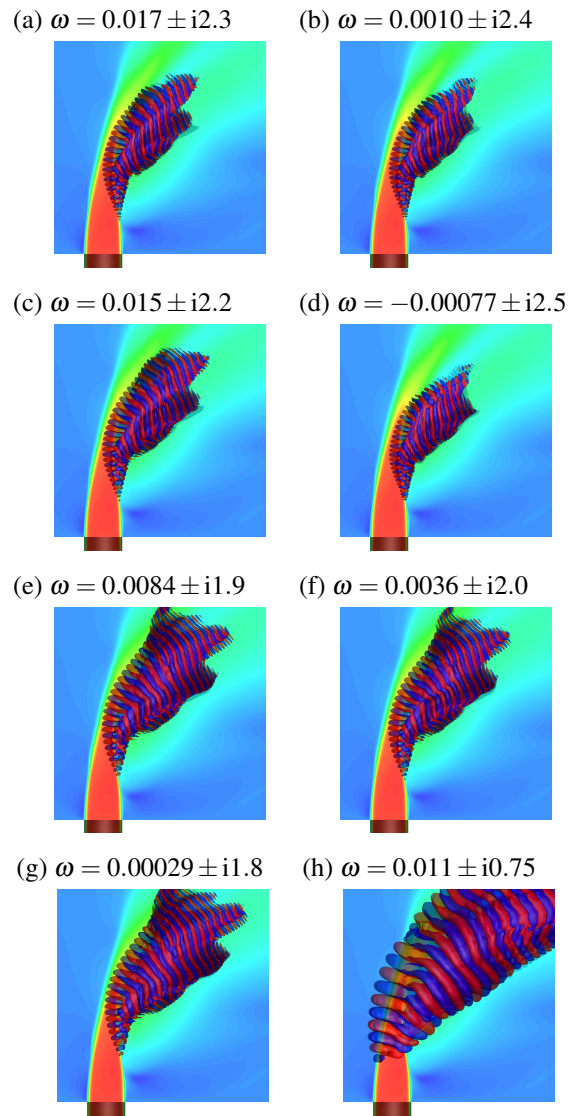
(a) $\omega = 0.017 \pm i2.3$ (b) $\omega = 0.0010 \pm i2.4$

(c) $\omega = 0.015 \pm i2.2$ (d) $\omega = -0.00077 \pm i2.5$

(e) $\omega = 0.0084 \pm i1.9$ (f) $\omega = 0.0036 \pm i2.0$

(g) $\omega = 0.00029 \pm i1.8$ (h) $\omega = 0.011 \pm i0.75$

Figure 4. Real part of the eigenmodes for case $R4$ are shown with positive and negative isocontours of $\tilde{u}$ and $\bar{v}$ contours of the base state in the background. Modes (a-g) correspond to the higher frequency downstream shear-layer modes. Mode (h) is associated with the upstream shear-layer.
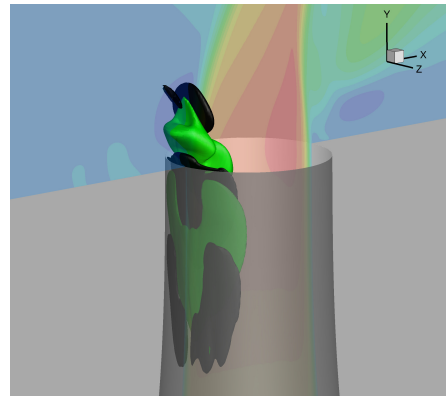

Figure 5. Real part of the adjoint eigenmode for case $R2$ is shown with positive and negative isocontours of $\tilde{u}$ and $\bar{v}$ contours of the base state int he background. The eigenmode has an associated non-dimensional eigenvalue $\omega = 0.050 \pm i0.61$, which coincides with the direct eigenmode and provides sensitivity information
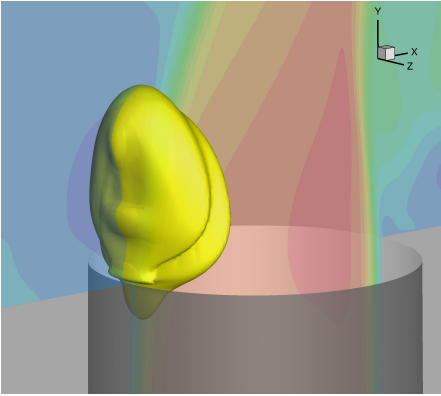
Figure 6. The wavemaker associated with the upstream shear-layer direct and adjoint eigenmodes. This highlights the most sensitive regions to localized feedback.

REFERENCES

Åkervik, E., Brandt, L., Henningson, D. S., Hœpffner, J., Marxen, O. & Schlatter, P. 2006 Steady solutions of the Navier-Stokes equations by selective frequency damping. *Physics of Fluids* **18** (6).

Arnoldi, W. E. 1951 The principle of minimized iteration in the solution of the matrix eigenproblem. *Quarterly of Applied Mathematics* **9**, 17–29.

Babu, P. C. & Mahesh, K. 2004 Upstream entrainment in numerical simulations of spatially evolving round jets. *Physics of Fluids* **16** (10), 3699–3705.

Bagheri, S., Schlatter, P., Schmid, P. J. & Henningson, D. S. 2009 Global stability of a jet in crossflow. *Journal of Fluid Mechanics* **624**, 33–44.

Crighton, D. G. & Gaster, M. 1976 Stability of slowly diverging jet flow. *Journal of Fluid Mechanics* **77**, 397–413.

Davitian, J., Hendrickson, C., Getsinger, D., M'Closkey, R. T. & Karagozian, A. R. 2010 Strategic Control of Transverse Jet Shear Layer Instabilities. *AIAA Journal* **48** (9), 2145–2156.

Eiff, O. S., Kawall, J. G. & Keffer, J. F. 1995 Lock-in of vortices in the wake of an elevated round turbulent jet in a crossflow. *Experiments in Fluids* **19** (3), 203–213.

Fric, T. F. & Roshko, A. 1994 Vortical structure in the wake of a transverse jet. *Journal of Fluid Mechanics* **279**, 1–47.

Hill, D. C. 1995 Adjoint systems and their role in the receptivity problem for boundary layers. *Journal of Fluid Mechanics* **292** (-1), 183.

Huerre, P. & Monkewitz, P. A. 1985 Absolute and convective instabilities in open shear layers. *Journal of Fluid Mechanics* **159**, 151–168.

Iyer, P. S. & Mahesh, K. 2016 A numerical study of shear layer characteristics of low-speed transverse jets. *Journal of Fluid Mechanics* **790**, 275–307.

Jordan, Peter & Colonius, Tim 2013 Wave Packets and Turbulent Jet Noise. *Annual Review of Fluid Mechanics* **45** (1), 173–195.

Kamotani, Y. & Greber, I. 1972 Experiments on a Turbulent Jet in a Cross Flow. *AIAA Journal* **10** (11), 1425–1429.

Karagozian, A. R. 2010 Transverse jets and their control. *Progress in Energy and Combustion Science* **36** (5), 531–553.

Kelso, R. M., Lim, T. T. & Perry, A. E. 1996 An experimental study of round jets in cross-flow. *Journal of Fluid Mechanics* **306**, 111–144.

Kelso, R. M. & Smits, A. J. 1995 Horseshoe vortex systems resulting from the interaction between a laminar boundary layer and a transverse jet. *Physics of Fluids* **7** (1), 153–158.

Krothapalli, A., Lourenco, L. & Buchlin, J. M 1990 Separated flow upstream of a jet in a crossflow. *AIAA Journal* **28** (3), 414–420.

Mahesh, K. 2013 The Interaction of Jets with Crossflow. *Annual Review of Fluid Mechanics* **45** (1), 379–407.

Mahesh, K., Constantinescu, G. & Moin, P. 2004 A numerical method for large-eddy simulation in complex geometries. *Journal of Computational Physics* **197** (1), 215–240.

Margason, R. J. 1993 Fifty Years of Jet in Cross Flow Research. In *Advisory Group for Aerospace Research & Development Conference 534*, pp. 1–41. Winchester, United Kingdom.

M'Closkey, R. T., King, J. M., Cortelezzi, L. & Karagozian, A. R. 2002 The actively controlled jet in crossflow. *Journal of Fluid Mechanics* **452** (2002), 325–335.

McMahon, H. M., Hester, D. D. & Palfery, J. G. 1971 Vortex shedding from a turbulent jet in a cross-wind. *Journal of Fluid Mechanics* **48** (1), 73–80.

Megerian, S., Davitian, J., Alves, L. S. de B. & Karagozian, A. R. 2007 Transverse-jet shear-layer instabilities. Part 1. Experimental studies. *Journal of Fluid Mechanics* **593**, 93–129.

Moussa, Z. M., Trischka, J. W. & Eskinazi, D. S. 1977 The near field in the mixing of a round jet with a cross-stream. *Journal of Fluid Mechanics* **80** (1), 49–80.

Muppidi, S. & Mahesh, K. 2005 Study of trajectories of jets in crossflow using direct numerical simulations. *Journal of Fluid Mechanics* **530**, 81–100.

Muppidi, S. & Mahesh, K. 2007 Direct numerical simulation of round turbulent jets in crossflow. *Journal of Fluid Mechanics* **574**, 59–84.

Muppidi, S. & Mahesh, K. 2008 Direct numerical simulation of passive scalar transport in transverse jets. *Journal of Fluid Mechanics* **598**, 335–360.

Peplinski, A., Schlatter, P. & Henningson, D. S. 2015 Global stability and optimal perturbation for a jet in cross-flow. *European Journal of Mechanics - B/Fluids* **49**, 438–447.

Pope, S. B. 2000 *Turbulent Flows*, 1st edn. Cambridge Univesity Press.

Sau, R. & Mahesh, K. 2007 Passive scalar mixing in vortex rings. *Journal of Fluid Mechanics* **582**, 449.

Sau, R. & Mahesh, K. 2008 Dynamics and mixing of vortex rings in crossflow. *Journal of Fluid Mechanics* **604**, 389–409.

Smith, S. H. & Mungal, M. G. 1998 Mixing, structure and scaling of the jet in crossflow. *Journal of Fluid Mechanics* **357** (1998), 83–122.